



Shiraz University
Faculty of Agriculture

PhD Thesis
In Water Science and Engineering

**GENERALIZED THREE-DIMENSIONAL CURVILINEAR
NUMERICAL MODELING OF LAMINAR AND TURBULENT
FREE-SURFACE FLOWS IN A VORTEX SETTLING BASIN**

By:

ALI NAGHI ZIAEI

Supervised by:

A.R. KESHAVARZI, PhD

H. EMDAD, PhD

July 2007

1387 / 7 / 10

دانشگاه شیراز
فصل کشاورزی

۸۲۳۱۷

Handwritten signature



دانشکده کشاورزی

پایان نامه دکتری
در رشته علوم و مهندسی آب

مدل سازی جریانهای آرام و متلاطم همراه با سطح آزاد در حوضچه
رسوبگیر گردابی

توسط:

علی نقی ضیائی

اساتید راهنما:

دکتر علیرضا کشاورزی

دکتر همایون امداد

تیرماه ۱۳۸۶

۴۶۳۱۷

۱۳۸۷ / ۱۷ / ۱۵

کتابخانه مرکزی
دانشگاه شاهرز

IN THE NAME OF GOD

**GENERALIZED THREE-DIMENSIONAL CURVILINEAR NUMERICAL
MODELING OF LAMINAR AND TURBULENT FREE-SURFACE
FLOWS IN A VORTEX SETTLING BASIN**

BY:

ALI NAGHI ZIAEI

Ph.D. THESIS

SUBMITTED TO THE OFFICE OF VICE-CHANCELLOR FOR GRADUATE
STUDIES IN PARTIAL FULFILLMENT OF THE REQUIREMENTS FOR THE
DEGREE OF DOCTOR OF PHILOSOPHY (PhD)

IN

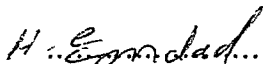
**WATER SCIENCE AND ENGINEERING
SHIRAZ UNIVERSITY
SHIRAZ, ISLAMIC REPUBLIC OF IRAN**

EVALUATED AND APPROVED BY THE THESIS COMMITTEE AS:

EXCELLENT



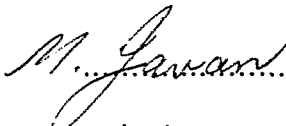
A. R. KESHAVARZI, PhD, ASSOCIATE PROF. OF WATER
SCIENCE AND ENGINEERING (CHAIRMAN)



H. EMDAD, PhD, ASSISTANT PROF. OF MECHANICAL
ENGINEERING (CHAIRMAN)

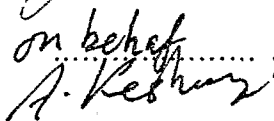


E. GOSHTASBI RAD, PhD, ASSISTANT PROF. OF
MECHANICAL ENGINEERING



M. JAVAN, PhD, ASSOCIATE PROF. OF WATER SCIENCE AND
ENGINEERING

on behalf



J. M. McDONOUGH, PhD, PROF. OF MECHANICAL
ENGINEERING AND MATHEMATICS, UNIVERSITY
OF KENTUCKY, USA

JULY 2007

Dedication

*This dissertation is dedicated, with great affection and
gratitude, to my wife*

ACKNOWLEDGMENTS

Special thanks to Allah who helped me throughout my life and particularly facilitated the progress of this study. Then I would like to express my sincere gratitude and admiration to my advisors, Dr. A. R. Keshavarzi and Dr. H. Emdad, for their invaluable guidance, encouragements and continuous support in the course of this study.

I would also like to appreciate the thesis committee members; Dr. E. Goshtasbi Rad, Dr. M. Javan, and Dr. J. M. McDonough, for their valuable comments, suggestions and supports to improve this thesis to its final form.

I also wish to express my appreciation to the faculty and staff of Water Engineering Department and Mechanical Engineering Department of Shiraz University, particularly Dr. M. M. Alishahi, Dr. Abouali, and HPCC staff, Mr. Khajeh and Ms. Falizi. I honored this study accomplished by kindly collaboration of Water Engineering and Mechanical Engineering Departments of Shiraz University which will hopefully flourish in future.

I specially acknowledge Dr. A. H. Nikseresht due to his valuable comments and suggestions during the development of the computer code.

I also thank the University of Kentucky Computing Center for providing access to the HP SuperDome SMP for some of computations performed during residence of the author as a visiting student at this university.

I am also very thankful to Dr. M. J. Abedini (referee), and Dr. M. J. Zamiri (representative of vice-chancellor for graduate studies) for all of their valuable comments and insights regarding my dissertation.

I would like to take this opportunity to express my appreciation to my sincere friends, Dr. A. Rasoulzadeh, Mr. A. R. Soltani Toudeshki, and Mr. A. Rabiee who helped me kindly during my PhD studies.

I would also like to take this opportunity to express my appreciation and thanks to my family and my wife's family who really provided me vision, hope and support to pursue my goals.

Finally, I would especially like to express my admiration and appreciation to my wife, F. Kalalinia, for her encouragement, understanding, patience and endless support that have made my life full of love, attraction and enjoyment.

ABSTRACT

GENERALIZED THREE-DIMENSIONAL CURVILINEAR NUMERICAL MODELING OF LAMINAR AND TURBULENT FREE-SURFACE FLOWS IN A VORTEX SETTLING BASIN

BY

ALI NAGHI ZIAEI

A three-dimensional numerical model has been developed to study the complex flow situations with air-water interface in a vortex settling basin. This model is based on solving Navier–Stokes (N.–S.) equations. For turbulence modeling, the Reynolds Averaged Navier–Stokes (RANS) equations were adopted. The standard $k-\varepsilon$ and $k-\omega$, were used to provide the information of turbulent eddy viscosity. A computer code was developed to solve above equations using finite volume approach in general curvilinear coordinates. The well-known SIMPLE algorithm was implemented to solve N.–S. or RANS equations. The free-surface motion is tracked by using piecewise linear volume of fluid (VOF) method.

The different parts of the numerical model were first validated by a number of laminar and turbulent single phase flows. Then free-surface tracking approach was verified using some simple analytical flow fields. The free-surface coupled with the equations of motion was also validated using a laminar liquid jet filling a thin rectangular mould. Then the code was applied to model some laminar and turbulent free-surface flows including a 3-D dam-break wave striking with a square cylinder, a hydraulic jump with different upstream Froude numbers and the water entry of a sphere with constant velocity. In order to study the flow field in the vortex settling basin (VSB), first a simplified cubic VSB was considered and

its outlet boundary conditions were investigated. Vorticity open boundary condition was introduced and applied for the outlets of this simplified geometry and advantages of this kind of BC were discussed. A preliminary assessment of the turbulence model performance in this geometry was then conducted.

Finally the code was used to study the unsteady flow behavior in a circular cylindrical VSB with a central clock-wise vortex. However, to keep the problem tangible and to save the computational time, only the flow filed inside the basin were modeled and the inlet channel omitted from the computational domain and an overflow weir was considered at the beginning of outlet channel. The detailed discussions about complex three-dimensional flow patterns, velocity fields, and free-surface deformations in the cylindrical VSB have been presented and discussed. These helped to shed more light on the very complicated flow structure in a VSB.

Table of Contents

CHAPTER 1	1
Introduction	1
1.1. Background and Literature Survey	3
1.2. Review of Turbulence Closure Models for RANS Equations	10
1.3. Free Surface Simulation	13
1.4. Scope and Structure of Present Study	15
CHAPTER 2	17
Formulations	17
2.1. Navier–Stokes Equations	17
2.1.1. Surface Tension	18
2.1.2. Initial and Boundary Conditions	19
2.1.2.1. Inflow Boundary Conditions	19
2.1.2.2. Outflow Boundary conditions	20
2.1.2.2.1. Tangential velocity component boundary conditions	21
2.1.2.2.2. Vorticity transport equation	22
2.1.2.2.3. Boundary condition for pressure and normal component of velocity	22
2.2. Turbulence Modeling	23
2.2.1. $k-\epsilon$ Model	25
2.2.2. $k-\omega$ Model	25
2.2.3. Initial Conditions	26
2.2.4. Inflow Boundary Conditions	26
2.2.5. Turbulence Properties at the OBs	27
2.2.6. Wall Function	27
CHAPTER 3	30
Numerical Implementation	30
3.1. Dimensionless Parameters	30

3.2. Finite-Volume Discretization Method on a Cartesian Grid.....	30
3.2.1. Discretization Schemes.....	33
3.2.1.1. The Power-Law Scheme.....	34
3.2.1.2. The QUICK Scheme.....	34
3.3. Discretization of N.–S. Equations in a Cartesian Grid.....	35
3.4. Finite-Volume Discretization in Curvilinear Coordinates.....	37
3.4.1. Discretization of the Non-orthogonal Terms.....	40
3.5. Discretization of the N.–S. Equations in Curvilinear Coordinates.....	42
3.5.1. Discretization of the Momentum Equations.....	43
3.5.2. Discretization of the Continuity Equation.....	45
3.6. Interface Kinematics.....	46
3.6.1. VOF Equations.....	46
3.6.2. Volume-Tracking Algorithm.....	47
3.6.2.1. Interface Normal Estimation.....	48
3.6.2.1.1. Centered-differencing (CD).....	48
3.6.2.1.2. Efficient least squares VOF interface reconstruction algorithm (ELVIRA).....	48
3.6.2.2. Interface Plane Intercept Estimation.....	51
3.6.2.3. Advection of the Interface.....	52
3.7. Numerical Implantation of Turbulence Models.....	54
3.7.1. Wall Function Implantation.....	55
3.7.1.1. Wall-Normal Velocity.....	56
3.7.1.2. Turbulence Parameters.....	57
CHAPTER 4.....	58
Numerical results.....	58
4.1. Model Testing.....	58
4.1.1. Laminar Flow Test Cases.....	58
4.1.1.1. The Laminar Flow Field in a 3-D Rectangular Duct.....	58
4.1.1.2. 3-D Lid-Driven Cavity.....	60
4.1.1.3. Developing Laminar Flow in a Pipe.....	63
4.1.1.4. Flow Past a Sphere.....	65

4.1.2. Free-Surface Testing.....	73
4.1.2.1. Validation on Simple Two-Fluid Advection Tests.....	73
4.1.2.2. Simulation of Viscous Two Fluid Interfacial problems.....	78
4.1.3. Developing Turbulent Flow in a Rectangular Duct.....	80
4.2. Model Applications.....	84
4.2.1. 3-D Dam-Break Waves Interacting with a Square Cylinder	84
4.2.1.1. Experimental and Numerical Setup	85
4.2.1.2. Comparison of Experimental Data and Numerical Results	86
4.2.1.2.1. N.-S. equations results	87
4.2.1.2.2. Turbulent results	93
4.2.2. The Hydraulic Jump.....	95
4.2.3. Water Entry of a Sphere with a Constant Velocity.....	101
4.2.4. Vortex Settling Basin.....	103
4.2.4.1. A simplified vortex Settling Basin Problem	103
4.2.4.1.1. Numerical setup	104
4.2.4.1.2. Laminar flow results	105
4.2.4.1.3. Preliminary assessment of the turbulence models	118
4.2.4.2. A Real Vortex Settling Basin Problem	127
4.2.4.2.1. VSB numerical setup	127
4.2.4.2.2. Numerical results	129
CHAPTER 5.....	137
Conclusions and Future works.....	137
5.1 Summary and Conclusions	137
5.2. Recommendations for Further Studies	139
REFERENCES.....	141

LIST OF Figures

Figure 1.1. Schematic diagram of a vortex settling basin (left) and the simplified model (right)	2
Figure 1.2. A schematic diagram of the clockwise model presented by Paul <i>et al.</i> (1991)	4
Figure 1.3. A schematic diagram of the counter-clockwise model presented by Paul <i>et al.</i> (1991).	4
Figure 1.4. A schematic diagram of the model presented by Ziaei (2000).	6
Figure 1.5. (a) Plan view of clockwise model; (b) Longitudinal section of clockwise geometrical model (after Athar <i>et al.</i> , 2002.).	7
Figure 1.6. (a) Plan view of counter-clockwise geometrical model; (b) Longitudinal section of counter-clockwise geometrical model (after Athar <i>et al.</i> , 2002).	7
Figure 3.1. A portion of the 2-D grid and related nomenclature used in the FVM, notice that "T" and "B" denote top and bottom values in a 3-D grid.	32
Figure 3.2. 2-D illustration of staggered-grid control volumes.	36
Figure 3.3. Illustration of the required physical geometric quantities for a control cell.	38
Figure 3.4. Illustration of discretization of cross-derivatives.	41
Figure 3.5. Illustration of the velocity expansion in 2-D local tangential basis vectors.	43
Figure 3.6. A general control volume with seven unknowns.	43
Figure 3.7. Illustration of using 3-D ELVIRA to find interface normal vector.	50
Figure 3.8. The region contained within the right parallelepiped ABCDEFGH and also below planar surface LMNK.	52
Figure 3.9. Lagrangian advection of the interface along the x -direction: (a) interface reconstruction in the central cell before advection; (b) contributions along the x -direction of the central cell after advection.	54
Figure 3.10. Illustration of wall function implementation in a cell located	56

adjacent to the wall.	
Figure 4.1. Stream wise velocity profile at the center line of a rectangular duct	60
Figure 4.2. The streamlines shown on three orthogonal planes through the center of the 3-D lid-driven cavity at $Re = 400$. The arrow indicates the location and direction of the driven lid.	61
Figure 4.3. Comparison of calculated u -velocity along the vertical centerline of the 3-D lid-driven cavity at $Re = 400$.	61
Figure 4.4. Comparison of calculated u -velocity along the vertical centerline of the 3-D lid-driven cavity with Ham <i>et al.</i> (2002) results.	62
Figure 4.5. Illustration of the grid used to compute the laminar flow field in a pipe.	64
Figure 4.6. Comparison between numerical and analytical streamwise velocity profile at the centerline of a pipe at $Re = 100$ in a well developed region of the pipe.	64
Figure 4.7. A 66^3 -cell grid shown on three orthogonal planes through the center of the sphere (left) and zoomed grid on the central plane along x -direction (right).	66
Figure 4.8. Computed axisymmetric streamlines past the sphere reported by Johnson and Patel (1999): (a) $Re = 50$; (b) $Re = 100$; (c) $Re = 150$; (d) $Re = 200$.	67
Figure 4.9. Flow geometry versus Reynolds number reported by Johnson and Patel (1999): (a) polar separation angle Θ_s ; (b) separation length x_s ; (c) vortex position (x_c, y_c) .	68
Figure 4.10. Computed axisymmetric streamlines past the sphere: (a) $Re = 10$; (b) $Re = 20$; (c) $Re = 50$; (d) $Re = 100$; (e) $Re = 150$; (f) $Re = 200$; (g) $Re = 250$.	69
Figure 4.11. Separation length x_s versus Reynolds number obtained using current study superposed on the Figure 4.9.	71
Figure 4.12. Drag coefficient versus Reynolds number.	72
Figure 4.13. Contours of the pressure coefficient, C_P ; (a) reported by Johnson and Patel (1999), and (b) the current results for $Re = 200$.	72

Figure 4.14. Performance of a piecewise constant tracking method in translating an initially cubic fluid body on a 32^3 grid. Reconstructed interfaces are shown for the body (a) before translating, (b) after being translated at 45 degree for a distance of one object diagonal, and (c) after being returned to its initial position.	75
Figure 4.15. Reconstructed interfaces for an initially circular cylinder (a) before translation one grid spacing in x direction and (b) after being returned to its initial position.	76
Figure 4.16. Reconstructed interfaces for a cubic fluid body during rotation around x axis using CD method.	77
Figure 4.17. The reconstructed circle affected by a single vortex using ELVIRA.	78
Figure 4.18. Geometry of a rectangular plate.	79
Figure 4.19. Flow front positions for filling a rectangular plate for $Re = 2000$ (left column) and $Re = 0.2$ (right column).	80
Figure 4.20. Flow development along axis of square duct. Data: +, Melling (1975), $Re = 42,000$; o, Gessner and Emery (1981), $Re = 250,000$ (reported by Demuren and Rodi, 1984); current study $Re = 65,000$ (Green thick solid line).	82
Figure 4.21. Streamwise velocity component profile at different x/D in the duct centerline using two different grid sizes and implementing two discretization schemes in momentum equations and two different turbulence model for $Re = 65,000$.	83
Figure 4.22. The predicted turbulent kinetic energy (using $k-\varepsilon$ model) profile at different x/D in the duct centerline using two different grid sizes for $Re = 65,000$.	83
Figure 4.23. The numerical setup for dam-break wave interacting with a square cylinder.	86
Figure 4.24. Snapshots of the free surface elevation obtained by solving nonlinear $k-\varepsilon$ turbulence model conducted by Wu (2004) (left column) and the N.-S. equations in the current study (right column).	88

Figure 4.25. The time-history wave impact on a square cylinder reported by Wu (2004). The numerical solutions of force on the square cylinder were validated with experimental data. The dot symbols are four sets of experimental data.	92
Figure 4.26. The time-history wave impact on a square cylinder predicted by solving the N.-S. equations (thick solid blue line) superposed on numerical and experimental results reported by Wu (2004).	93
Figure 4.27. The time-history wave impact on a square cylinder predicted by standard $k-\varepsilon$ using two different grid size; $84 \times 30 \times 44$ -cell (thin dotted blue line) and $104 \times 30 \times 48$ -cell (thick solid red line) superposed on numerical and experimental results reported by Wu (2004).	94
Figure 4.28. The time-history of velocity in a specific location upstream of the cylinder, predicted by standard $k-\varepsilon$ using a $104 \times 30 \times 48$ -cell grid (dotted green line) and N.-S. equations (thick solid red line) superposed on numerical and experimental results reported by Wu (2004).	95
Figure 4.29. Jump forms related to Froude number (USBR, 1987).	97
Figure 4.30. Snapshots of downward propagation of waves generated by a hydraulic jump with $Fr = 2.0$.	99
Figure 4.31. Snapshots of downward propagation of waves generated by a hydraulic jump with $Fr = 2.5$.	100
Figure 4.32. The velocity vector and free-surface at a similar snapshot on the central vertical plane of the channel for (a) $Fr = 2$ and (b) $Fr = 2.5$.	101
Figure 4.33. Impact jetting for a unit diameter sphere enters to the water surface at constant velocity $U = 1 \text{ m s}^{-1}$.	103
Figure 4.34. Typical grid cell on an outflow boundary.	105
Figure 4.35. Velocity component profiles, computed using QUICK scheme, along lines: (a) $y=0.5, z=0.5$; (b) $x=0.5, y=0.5$; (c) $x=1.0, y=0.5$; and (d) $x=0.5, y=0.0$.	108
Figure 4.36. Velocity vectors: (a) adjacent to bottom outlet; and (b) at the outlet channel.	109
Figure 4.37. Flow variable profiles normal to: (a) outlet channel; and (b)	

bottom outlet.	110
Figure 4.38. Comparison between velocity profiles at the outlets, computed using two different methods to handle normal velocity component at the image points.	111
Figure 4.39. Trajectories of fluid particles released from various points in the vortex settling basin.	113
Figure 4.40. Streamlines projected on planes: (a) $y = 0.0125$; (b) $y = 0.0625$; (c) $y = 0.5$; (d) $x = 0.25$; (e) $x = 0.5$; and (f) $x = 0.75$.	114
Figure 4.41. Streamlines projected on constant- z planes: (a) $z = 0.25$; (b) $z = 0.5$; and (c) $z = 0.75$.	115
Figure 4.42. Velocity profiles transformed to cylindrical coordinates along lines: (a) $y = 0.5, z = 0.5$; (b) $x = 0.5, y = 0.5$; (c) $y = 0.25, z = 0.5$; (d) $x = 0.5, y = 0.25$; (e) $y = 0.0625, z = 0.5$; and (f) $x = 0.5, y = 0.0625$. Velocity profiles transformed to the cylindrical coordinates along lines: (g) $y = 0.0, z = 0.5$; and (h) $x = 0.5, y = 0.0$.	117
Figure 4.43. Some predicted streamlines started from inlet in the vortex settling basin using $k-\omega$ model.	119
Figure 4.44. Streamlines projected on horizontal planes: (a) $y = 0.5$ and (b) $y = 0.025$, predicted using $k-\omega$ model.	120
Figure 4.45. Streamlines projected on vertical planes: (a) $z = 0.25$; (b) $z = 0.5$; (c) $z = 0.75$; (d) $x = 0.25$; (e) $x = 0.5$; and (f) $x = 0.75$, predicted using $k-\omega$ model.	121
Figure 4.46. Velocity vector at open boundaries computed using $k-\omega$ model.	122
Figure 4.47. The turbulent velocity profiles transformed to cylindrical coordinates along: (a) $y = 0.5, z = 0.5$; (b) $x = 0.5, y = 0.5$; (c) $y = 0.25, z = 0.5$; (d) $x = 0.5, y = 0.25$; (e) $y = 0.0, z = 0.5$; and (f) $x = 0.5, y = 0.0$.	123
Figure 4.48. Contour plots of: (a) k and (b) ω on plane $y = 0.5$ computed using $k-\omega$ model.	125
Figure 4.49. Contour plots of: (a) k and (b) ε on plane $y = 0.5$ computed using $k-\varepsilon$ model.	126

- Figure 4.50. A sketch of the VSB, inlet channel and overflow weir used to setup the numerical model. The dark color shows the considered initially static water surface. 128
- Figure 4.51. A grid used to solve the N.-S. Equations in a cylindrical VSB ($72 \times 32 \times 72$ -cell in x , y , and z direction). 129
- Figure 4.52. The developing water surface in a vortex settling basin at different time levels, predicted by the present numerical model. 130
- Figure 4.53. Trajectories of fluid particles released from various points in the inlet of the cylindrical vortex settling basin. 131
- Figure 4.54. Streamlines projected on horizontal planes: (a) $y = 0.2$, (b) $y = 0.1$, and (c) $y = 0.06$ m. 132
- Figure 4.55. Streamlines projected on: (a) x - y , and (b) y - z planes in the centerline of the basin. The dark color shows the water surface profile. 133
- Figure 4.56. Velocity profiles transformed to cylindrical coordinates along lines: (a) $y = 0.2$, $z = 0.0$; (b) $y = 0.1$, $z = 0.0$; and (c) $y = 0.06$, $z = 0.0$. U is the basin inlet velocity. 135
- Figure 4.57. Velocity profiles transformed to cylindrical coordinates along lines: (a) $y = 0.2$, $x = 0.0$; (b) $y = 0.1$, $x = 0.0$; and (c) $y = 0.06$, $x = 0.0$. U is the basin inlet velocity. 136

List of Tables

Table 4.1. Grid-function convergence test for the 3-D lid-driven Cavity	63
Table 4.2. L^1 Error norms and convergence rates for a cubic fluid body translated as its diagonal and returned to its initial position	74
Table 4.3. L^1 Error norms and convergence rates for a circular cylinder fluid body translated one grid spacing at two different angles using two different reconstructing algorithms	76
Table 4.4. Grid-function convergence test for the simplified vortex settling basin	106

Chapter 1

Introduction

Except for mountainous rivers or large dams, diverted water usually carries considerable amounts of sediment that produce problems in distribution networks. The sediment particles decrease the discharge capacity of conveyance canals, clog sprinklers and drippers, and erode canals and hydropower tunnel linings, penstocks and turbines. Moreover, they produce complication by necessity to clean away sediment deposited and arrange for their disposal, which are costly and time consuming.

To overcome the above problems, sediment removal devices are widely used. These devices are divided in two main categories: intermittent and continuous operation systems. Continuous systems utilize a fraction of the diverted flow to flush out the extracted sediment particles from the sediment chamber. These systems obviate the need to clean away the deposited sediment in the settling basin. A vortex settling basin (VSB) is a continuous flushing system which is used to remove sediment from diverted water. Since the size of a VSB is small, the construction cost of a VSB is just a fraction of the cost required for the construction of a classical settling basin to extract comparable particles (Mashauri, 1986). A schematic diagram of this device and a simplified model (to be employed in numerical simulations to be described below) was presented in Ziaei *et al.* (2007) and repeated here as Figure 1.1. A VSB is an efficient device that uses a vortex motion with vertical axis to remove sediment from water. In a VSB, flow is introduced tangentially into a cylindrical chamber having an orifice at the center of its bottom. The induced combined vortex (combination of free and forced vortices) within the chamber causes sediment particles that are heavier than water to move towards the periphery of the chamber due to centrifugal force. Secondary flows move the fluid layer near the basin floor toward the central orifice. Since the sediment particles move with the flow along a helical path, they have a settling length that is longer than the basin dimensions. This feature makes the VSB more efficient than ordinary settling tanks.

Elaborate studies were made on different properties of the VSB mostly by physical modeling. Therefore, our knowledge of VSB flow structure relies heavily on laboratory experiments and empirical or semi-empirical correlations. However, it is well known that laboratory experiments suffer from constraints on the range of applicable physical parameters and scaling effects, not to mention the cost associated with performing careful experiments. Due to recent rapid advancement of computational power, 3-D Navier–Stokes solvers to simulate flow in hydraulic structures have been developed. These numerical models have the potential to become useful research tools for better understanding the physical processes and engineering tools to design these structures.

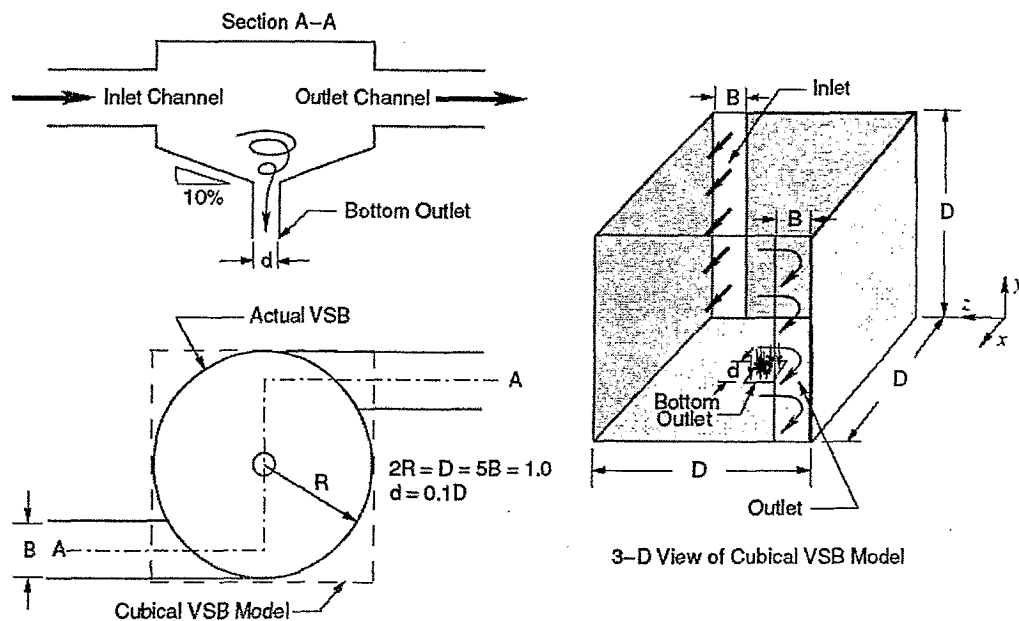


Figure 1.1. Schematic diagram of a vortex settling basin (left) and the simplified model (right).

In this study, a numerical tool which is able to simulate three-dimensional complex flow situations with air-water interfaces in a vortex settling basin will be developed. The accuracy of this numerical model will be examined and validated by different test cases in terms of turbulence characteristics, free surface profiles and velocity fields. Some useful results that are difficult to be measured by the experiments will be presented and discussed.